

The visibility study of S-T₊ Landau-Zener-Stückelberg oscillations without applied initialization

G. Granger, G. C. Aers, S. A. Studenikin, A. Kam, P. Zawadzki, Z. R. Wasilewski, and A. S. Sachrajda*
National Research Council Canada, Ottawa, ON Canada K1A 0R6

Probabilities deduced from quantum information studies are usually based on averaging many identical experiments separated by an initialization step. Such initialization steps become experimentally more challenging to implement as the complexity of quantum circuits increases. To better understand the consequences of imperfect initialization on the deduced probabilities, we study the effect of not initializing the system between measurements. For this we utilize Landau-Zener-Stückelberg oscillations in a double quantum dot circuit. Experimental results are successfully compared to theoretical simulations.

PACS numbers: 73.63.Kv, 73.23.-b, 73.23.Hk

I. INTRODUCTION

Spin qubits have generated a lot of interest recently in systems of single, double quantum dots (DQDs),¹⁻⁴ triple quantum dots (TQDs),⁵⁻⁹ and two coupled DQDs.¹⁰

Frequently probabilities are obtained from averaging thousands of individual measurements, with each measurement separated by an initialization pulse. For example, to initialize into a singlet state a pulse can be applied to an appropriate location in the stability diagram where a dot electron will be replaced by one from the leads with the appropriate spin (see, for instance, the supplementary information from Ref.¹¹). Such initialization pulses can also be used in larger TQD systems,⁹ but it is expected to be more difficult to continue implementing this technique in more complex quantum dot circuits due to the isolation of the inner dot electrons. It is therefore important to understand the consequences and signatures of an imperfect initialization step on the oscillation visibility. Experiments and numerical calculations aimed at the quantitative confirmation of these qualitative predictions are therefore required. The observation that the visibility of coherent oscillations is qualitatively affected by the choice of pulse period in relation to the spin relaxation time T_1 is briefly discussed in Ref.¹².

Here, we study the effect of not initializing the system between measurements. For this we utilize Landau-Zener-Stückelberg (LZS) oscillations¹¹⁻¹⁹ in a double quantum dot circuit. In Section II, we describe the sample and the experimental setup used in the measurements. In Section III, we explain the physics behind the LZS oscillations, as this is crucial for the understanding of the main parts of the paper. Section IV shows the details pertaining to the model used for comparative theoretical calculation. The experimental and theoretical LZS oscillations are compared in Section V. The observation that the visibility of the oscillations can be optimized is included in Section VI, while a discussion of the effects due to the nuclear spins in the lattice is detailed in Section VII.

II. EXPERIMENTAL DETAILS

The device geometry is shown in Fig. 1(a).^{6,20} It is fabricated on a GaAs/AlGaAs heterostructure with a two-dimensional electron gas (2DEG) located 110 nm below the surface with a density of $2.1 \times 10^{11} \text{ cm}^{-2}$ and a mobility of $1.72 \times 10^6 \text{ cm}^2/\text{Vs}$. TiAu gate electrodes, patterned by electron-beam lithography, define the quantum dot potential profile and quantum point contacts (QPCs).²¹ Charge detection measurements are made with the left QPC, tuned to a conductance regime very sensitive to the local electrostatic environment, below $0.1 e^2/h$, using a lock-in technique with a typical $50 \mu\text{V}$ rms modulation. Short DC (rectangular) pulses of duration τ (defined prior to the Gaussian convolution) and period τ_m from two synchronized arbitrary waveform generators (Tektronix AWG710B) are applied to gates 1 and 2 via bias-tees to quickly change the dc voltages V_1 and V_2 by small increments δV_1 and δV_2 . As τ_m is orders of magnitude larger than τ , τ_m is called the measurement time in practice. The τ_m values will be varied in such a way to span the regime where the measurement time is much longer than the spin relaxation time T_1 (so the next initial state is the ground state) to the regime where the measurement time is smaller than T_1 (so incomplete relaxation provides either the excited state or the ground state as the next initial state). The pulse rise times are controlled by loading pulses that correspond to the numerical convolution between a rectangular pulse and a Gaussian function into the arbitrary waveform generators [Fig. 1(c)]. The experimentally measured resulting rise times are defined in the region from 10% to 90% of maximum amplitude. The magnetic field is applied parallel to the 2DEG. To reduce telegraphic noise issues the device is bias-cooled with 0.25 V on all gates from room to the base temperature of the dilution refrigerator.

We focus on the (2,0) and (1,1) regions of the stability diagram [Fig. 1(b)], where (N_L, N_C) represents the electronic configuration with the indicated number of electrons on the left and center quantum dots respectively. The device is a triple quantum dot lithographically; however, the measurements are made in a regime where the

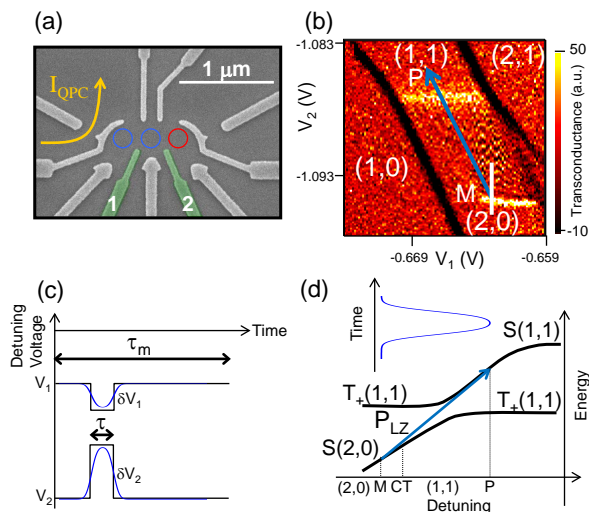


FIG. 1: (Color online) (a) Electron micrograph of a device similar to the one measured. The gates define the triple quantum dot potential and two QPCs used as charge detectors. The blue circles schematically indicate where the dots under study are located and the red shows the unused dot. Gates 1 and 2 receive short voltage pulses shown in (c) in addition to DC voltages V_1 and V_2 . The left QPC current I_{QPC} is used to detect the electron number, plot the stability diagram, and perform the spin readout. (b) Stability diagram from the measured transconductance of the left QPC in the V_1 - V_2 plane. The transconductance is the numerical derivative of the left QPC conductance with respect to V_2 . The electronic configurations are indicated, and LZS fringes are seen in the (2,0) region. The pulse size and direction are indicated by the blue arrow. M is the measurement point, while P is the maximum detuning point during the pulse. $(\delta V_1, \delta V_2) = (-5, 10)$ mV, $\tau = 16$ ns, $\tau_m = 2$ μ s, and $B = 80$ mT. The rise time is 8 ns. The initial detuning line relevant to the data in Fig. 3(a) is shown with a white line. (c) Schematic showing the definition of the rectangular pulses (black) and the resulting Gaussian-convoluted pulses used here (blue). τ is the pulse duration, while τ_m is the pulse period. The pulse amplitudes δV_1 and δV_2 applied to gates 1 and 2 are also indicated prior to the convolution. It is expected that for the rise times used here, the effective amplitude will be a little smaller than what is shown on the rectangular pulse. (d) Schematic of S- T_+ energy diagram as a function of detuning showing the anticrossing between S and T_+ . During the pulse, there is a Landau-Zener probability P_{LZ} of reaching the upper branch of the S- T_+ anticrossing. “CT” indicates the charge transfer line. Inset: Gaussian-convoluted pulse.

right dot is detuned away from this part of the stability diagram and plays no role in the measurements. The device therefore is an effective double quantum dot and the center quantum dot will be referred to as the right dot from now on.

The thick black lines in Fig. 1(b) are addition lines; the electron number in one of the dots changes by one whenever one of these lines is crossed. The upper yellow horizontal line in Fig. 1(b) is the charge transfer line be-

tween the (2,0) and (1,1) regions; whenever this line is crossed, an electron is transferred from the left dot to the right dot (or vice versa). The other features, including the lower yellow line, pertain to the presence of the pulse and will be described in the next section.

III. LANDAU-ZENER-STÜCKELBERG OSCILLATIONS

The experiments involve the creation of a superposition by passage through an anticrossing (analogous to a beam splitter), phase evolution, completing the interferometer by passing through the anticrossing a second time and then reading out the state. The required anticrossing occurs naturally in the scheme. The state of two electrons in the (2,0) or (1,1) electronic configurations can either be a spin 0 singlet or a spin 1 triplet. As a result of the magnetic field applied along the z direction and the sign of the electron g-factor in GaAs, the lowest energy triplet component is $T_+ = |\uparrow, \uparrow\rangle$. There exists a point in the (1,1) region of the stability diagram along the pulse detuning line where the S and T_+ states anticross. This is illustrated schematically in Fig. 1(d), where we ignore the other triplet components and the S(1,1)-S(2,0) anticrossing to focus on the particular anticrossing in which we are interested. For the full state spectrum the reader is referred to Ref.¹¹. This anticrossing between the S and T_+ states originates from spinflips mediated by the hyperfine interaction between the electron spins and the host lattice nuclear spins.¹¹ The confined electron spins experience an effective Overhauser magnetic field originating from the lattice nuclei. This is slightly different for electrons in the two dots, purely from statistical considerations, resulting in Overhauser field gradients. The interaction at the anticrossing is proportional to $g\mu_B\Delta B_{x,y}$, where g is the g-factor of conduction electrons in GaAs, μ_B is the Bohr magneton, and $\Delta B_{x,y}$ is the Overhauser field gradient perpendicular to the applied magnetic field.

The initial diabatic transition probability between the two eigenstates of the S- T_+ anticrossing, when applying a pulse which detunes the system through the anticrossing from (2,0) to (1,1), is given by

$$P_{LZ} = \exp \left\{ - \frac{(2\pi g\mu_B\Delta B_{x,y})^2}{\hbar \left| \frac{d}{dt}(E_+ - E_-) \right|} \right\} \quad (1)$$

where \hbar is Planck’s constant and E_+ and E_- refer to the eigenenergies of the two states involved in the S- T_+ anticrossing.¹¹ The key to creating a quantum superposition between S and T_+ is to allow the detuning to change at the appropriate speed, for which the Landau-Zener probability differs from zero. If the detuning changes extremely slowly, $P_{LZ} = 0$ as for an adiabatic process, while if the detuning changes extremely fast, $P_{LZ} = 1$ as for a fully diabatic process.

Once a quantum superposition is created, the relative phase difference $\Delta\phi$ between the two eigenstates

is given by the time integral of the detuning-dependent energy difference between these states, i.e. $\Delta\phi = \int_0^t (E_+ - E_-)dt'/\hbar$. At fixed initial detuning, increasing the pulse duration would lead to oscillations in the probability of finding either spin state, as $\Delta\phi$ increases linearly with the time spent at the end of the pulse in the (1,1) region. In this paper we vary the initial detuning while holding the pulse duration constant. The pulse duration of 16 ns was determined mainly by limitations due to the decoherence time T_2^* (which lies in the 5-15 ns range here) and the chosen pulse rise time (8 ns). The formula for $\Delta\phi$ still applies in the case of fixed pulse duration. As the initial detuning increases, the pulse goes further in the (1,1) region past the S- T_+ anticrossing, the energy difference $E_+ - E_-$ increases, and therefore the relative phase $\Delta\phi$ grows. This leads to oscillations in the probability of finding either spin state as a function of detuning. This describes the phase accumulation near the top part of the pulse, at largest detuning. This process needs to be integrated everywhere the pulse is past the anticrossing. Ideally P_{LZ} would be ~ 0.5 for optimum superposition. For the pulse and statistical inhomogeneous field gradient in these experiments, the initial value for P_{LZ} after passing through the anticrossing is, however, approximately $\sim 95\%$. The final part of the applied pulse detunes the system back through the anticrossing. P_{LZ} will once again change the quantum superposition of the already superposed states. In theory, it would be possible to apply a more complex train of pulses prior to commencing the phase evolution experiment to improve the degree of initial superposition, but the experiments and theory in this paper involve superpositions created by single pulses.

In the case of the S- T_+ anticrossing, the charge detector cannot distinguish the two spin states in the (1,1) region, as the underlying charge state is the same for both states. However, on passage through the anticrossing a second time and into the (2,0) region of the stability diagram, the S component evolves smoothly to the (2,0) ground state, while T_+ remains in the excited state with a (1,1) charge configuration since the triplet (2,0) is not energetically accessible. Thus after the pulse is complete, at the measurement point M in the (2,0) region, the resulting spin state information can be converted into charge information, a process referred to as spin-to-charge conversion,^{1,22} as the spin states map to different charge states there. The charge detector (a nearby quantum point contact) makes a measurement by effectively projecting the spin state on the S and T_+ basis states. In practice, the QPC conductance is averaged over $\sim 10^5$ identical pulses. The probability of returning in S after such an experiment depends upon many factors such as the effectiveness of the Landau-Zener process, the relaxation time, and decoherence time of the system.

Certain reported experiments have utilized an initialization step before every measurement in the averaged collection (e.g. Ref.¹¹) by adding a preliminary pulse toward one of the addition lines in the (2,0) region prior

to the detuning pulse described above. This allows for an exchange of an electron between the dot and the lead to achieve the desired singlet state. We call these IS experiments to differentiate them from experiments where there is no such pulse (NIS). In the latter case the resulting state at the end of the measurement is used as a starting point of the next pulse. The statistics over many pulses will still oscillate as a function of detuning. In this paper, we compare these two procedures.

We can infer the position of the S- T_+ anticrossing in the stability diagram from the position of the lower horizontal yellow line in the (2,0) region of the stability diagram in Fig. 1(b). When the measurement point M is on this yellow line, the tip of the pulse P reaches the S- T_+ anticrossing. Above this yellow line are fringes corresponding to LZS oscillations since in that regime the detuning pulse passes through the S and T_+ states anticrossing in the (1,1) region [see Fig. 1(b,d)]. The resolution is poor due to a small number of averages, but is sufficient to locate the region where LZS oscillations are present. Note that, in the stability diagram of Fig. 1(b), the QPC conductance data are numerically differentiated with respect to the V_2 gate voltage for an improved presentation. In all other graphs the QPC conductance data are normalized relative to the conductance step at the charge transfer line between (1,1) and (2,0) to get a probability of return in state S between 0 and 1.

IV. CALCULATIONS DETAILS

Throughout the paper we distinguish data with an initialization step and without initialization step. Let us explain what this means from the point of view of the calculations and the experiments. In the calculations, No Initialization Step (NIS) means that the final result for P(S) is the probability averaged over 1000 pulse sequences, where the final state (S or T_+) determined after any given pulse is the starting state for the next pulse. In the calculation, what we call the Initialization Step (or IS) is just the resulting P(S) after the first pulse, where the initial conditions prior to the pulse have been set theoretically to the singlet state. Experimentally, No Initialization Step (NIS) means we only apply the Gaussian-convoluted pulses and no other pulses.²³

The NIS repeat pulse scheme is simulated theoretically with the following model based on the solution of the time dependent density matrix.^{6,24} The system is initialized in the S state after which the first pulse is applied. During the measurement cycle the population is allowed to partially relax to the ground state with a decay time T_1 . At the end of each pulse cycle the state vector is then projected onto the charge basis to yield either S or T_+ occupation, which then defines the initial state for the next pulse cycle. As in experiment, P(S) is obtained as the fraction of measurements that find the system in the S state. Typically 1000 such cycles provide sufficient statistics to model the effects of relaxation and initial

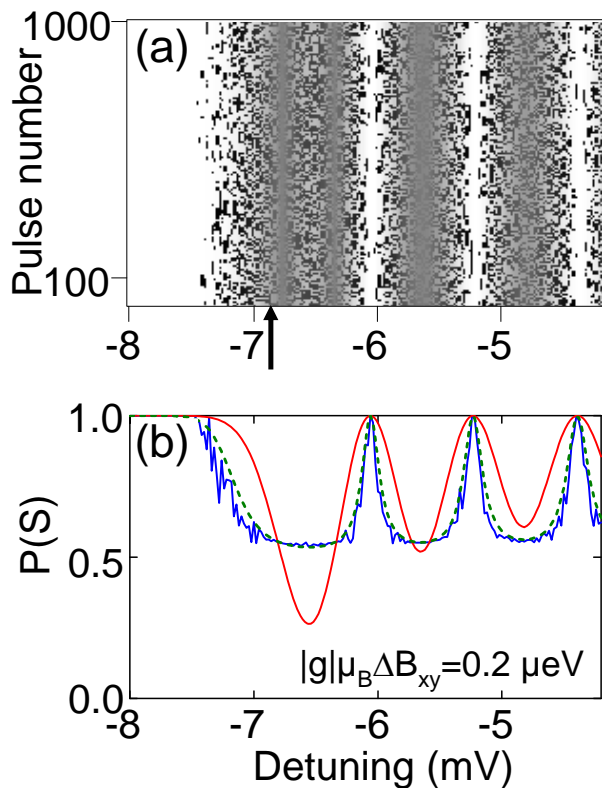


FIG. 2: (Color online) (a) Calculated 2D map of $P(S)$ vs. initial detuning for 1000 consecutive pulses. Black is $P(S)=0$ and white is $P(S)=1$. The arrow indicates where the S - T_+ anticrossing is observed on the initial detuning axis (as in the lower horizontal yellow line in Fig. 1(b)). (b) Calculated $P(S)$ vs. initial detuning for hyperfine splitting $|g|\mu_B\Delta B_{x,y}=0.2 \mu\text{eV}$ of the IS case (red). The blue curve is the NIS case from the average over 1000 pulse repeats. The green dashed curve is NIS derived from IS (see text).

state variation (typical experimental sequences involve 10^5 pulses). Since the measurement time after each pulse had a duration much greater than the pulse itself it was found impractical to include the measurement segment in the simulation. By the same token, however, almost all of the relaxation occurs during this measurement time when no other relevant time variation is present. Thus, the T_1 decay was not included explicitly in the density matrix and was instead added by means of an exponential term prior to each projection operation.

A typical 1000 cycle repeat of the calculated $P(S)$ vs. initial detuning scan is shown in Fig. 2(a) for a low value of $\tau_m/T_1 \sim 0.1$, where consequences of relaxation are less important, and a hyperfine splitting $|g|\mu_B\Delta B_{x,y}=0.2 \mu\text{eV}$, consistent with experimentally measured values for the hyperfine splitting.⁶ For a given initial detuning, the vertical axis shows the result of each consecutive measurement. For the same parameters, Fig. 2(b) shows the IS case from the first pulse response in red, and the NIS case from the averaged probability

over 1000 pulses in blue [averaging over the vertical direction in Fig. 2(a)].

It is instructive to derive the NIS result from the single pulse (IS) curve for $P(S)$ using an iterative approach. Here $P(S)$ serves as the starting estimate of the NIS probability of being measured in S . Due to symmetry it is also the probability, we call it P in this role, of a single pulse leaving the system in the state it started in, whether that state be S or T_+ . As can be seen from Eq. (1), the probability of diabatic transition depends only on the time derivative of the energy spacing and not on the choice of initial state (S or T_+). Likewise $(1-P)$ is the probability of a single pulse switching the final state from that in which it started. Under NIS conditions we can write a self-consistent condition for the total probability of measurement in the S state as the sum of the probability of starting in the S state and staying there after another pulse plus the probability of starting in the T_+ state and then switching during the pulse:

$$P(S) = P'(S)P + [1 - P'(S)](1 - P) \quad (2)$$

where $P'(S) = 1 - [1 - P(S)]e^{-\tau_m/T_1}$ accounts for the decay from T_+ to S over the pulse sequence.

This has an analytic solution for the NIS averaged probability of returning in S as

$$P'(S) = \frac{Pe^{-\tau_m/T_1} - 1}{(2P-1)e^{-\tau_m/T_1} - 1} \quad (3)$$

where P is the single pulse curve (red curve in Fig. 2(b)). The iterative formulation in the above analysis is a mathematical construction not to be confused with pulse repeats. As can be seen in Fig. 2(a), the statistical distribution of the pulse measurements in the numerical simulations do not vary from pulse to pulse. The above procedure gives the green dashed line in Fig. 2(b) which agrees well with the 1000 pulse repeat result. It also provides insight into the form of the NIS curve. Note, for example, that the expression for $P'(S)$ will always produce a value between 0.5 and 1.0, even from a $P(S)$ minimum below 0.5, as in Fig. 2(b). For $P=1$ we get $P'(S)=1$; for $P=0$ we get $P'(S)=1/(1+e^{-\tau_m/T_1})$ which gives 0.5 for small τ_m/T_1 and 1 for large τ_m/T_1 , i.e. $P'(S)$ lies between 0.5 and 1. More generally, when τ_m/T_1 is small, the result is always 0.5 for any value of P not exactly equal to 1. Thus, a cosine-like form for the single pulse P leads to a non-cosine-like NIS probability peaking sharply and having values >0.5 .

The oscillations in the IS case of Fig. 2(b) appear to become damped as initial detuning increases. This is due to the fact that P_{LZ} is optimal to create a superposition only near the S - T_+ anticrossing. At detunings further away from the anticrossing, $P_{LZ} \sim 95\%$ and the superposition contains less and less of T_+ hence the higher measured values of $P(S)$. To first order, the detuning period of the oscillations, T_e (in mV), along the detuning axis (i.e. along the ϵ axis) is inversely proportional to

$|d(E_+ - E_-)/d\epsilon|$ at the peak of the pulse (where most of the phase difference is accumulated). The detuning dependence of $E_+ - E_-$ is shown in Fig. 1(d). For instance, over detuning ranges where the eigenstates change approximately linearly with ϵ , the derivative will be a constant, so T_ϵ is constant. Therefore, equally spaced fringes along the detuning axis are expected as a function of detuning where $E_+ - E_-$ varies approximately linearly with ϵ (i.e. some distance away from the anticrossing).

The most prominent feature in the NIS case shown in Fig. 2(b) is that in narrow regions around where $P(S)=1$ in the IS case (red curve), the pulse averaged probability in the NIS case (blue curve) remains near unity. This is because the singlet that is measured after the first pulse becomes the initial and final state for all subsequent pulses so $P(S)\sim 1$. As the detuning is moved away from these points, the projection operation introduces more statistical cases where $P(S)=0$, and, in the regions where $P(S)$ is a minimum in the IS case, the minimum in the NIS case broadens and approaches 0.5 at this low $\tau_m/T_1\sim 0.1$. For the first minimum in the IS case that drops below 0.5, the probability in the NIS case is noisier but again averages towards 0.5 (the statistical average of these pure T_+ and S results after each pulse leads to $P(S)\sim 0.5$). This is true independently of detuning, so there is little appreciable damping in the $P(S)$ minima along the detuning axis in the NIS case.

V. LZS OSCILLATION AMPLITUDE DEPENDENCE ON PULSE PERIOD

The visibility of the LZS oscillations in $P(S)$ is expected to depend on the choice of pulse period τ_m and on the value of T_1 at the measurement point.¹² A few periods of LZS oscillations vs. initial detuning and τ_m are shown in Fig. 3(a). These oscillations are obtained by using a single Gaussian-convoluted rectangular pulse of a constant amplitude.^{6,11} The peak amplitude of each LZS oscillation decreases as τ_m increases due to the spin relaxation time T_1 . We extract T_1 as the value of τ_m where the peak amplitude decreases to 37% of its maximum value. We find that T_1 grows from 20 μs to 60 μs as initial detuning becomes more negative in Fig. 3(a). Because the spectrum of excited states changes with detuning as the DQD potential is deformed by the gate voltages, the inelastic decay mechanisms for the states also change, hence the triplet excited state relaxation time T_1 varies with detuning.

Figure 3(b) plots the results of a calculation in the NIS case that corresponds to the experimental case of Fig. 3(a). Our calculation is based on the model described above and in Refs. ^{6,24}. In the calculation, the detuning dependence of T_1 at the measurement point is not taken into account. The value used is $T_1=60 \mu\text{s}$. This explains why the three calculated LZS peak amplitudes decay in an identical fashion versus τ_m in contrast to the experimental results in Fig. 3(a) where T_1 does

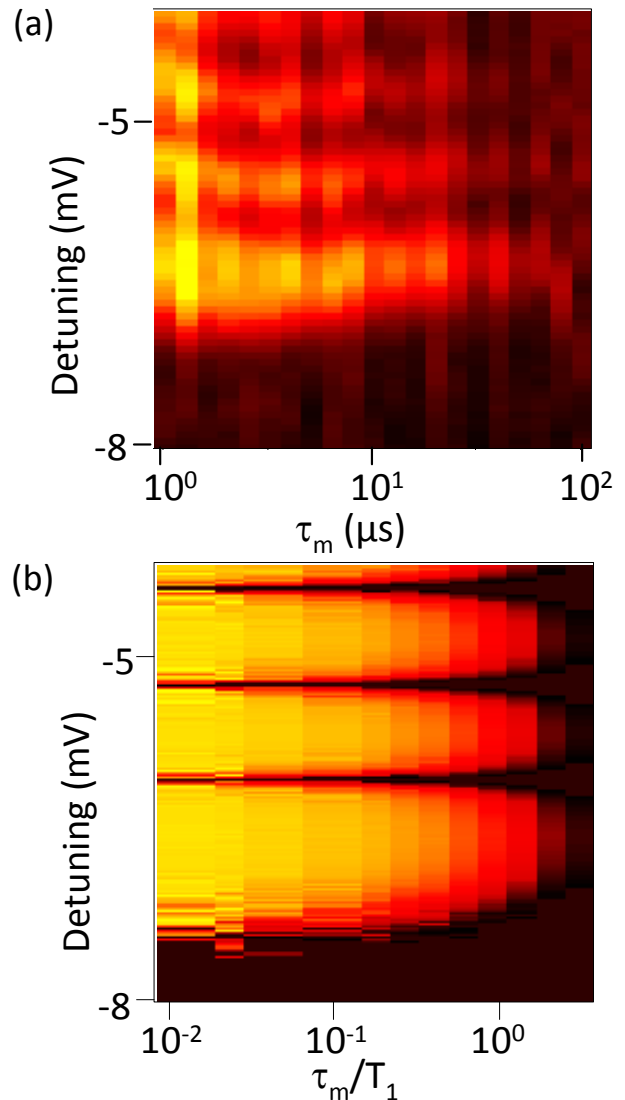


FIG. 3: (Color online) (a) LZS oscillations of $P(S)$ in the τ_m -initial detuning plane from the left QPC conductance (plane subtracted) taken along the white line from Fig. 1(b). The initial detuning is with respect to the position of the charge transfer line in Fig. 1(b). $(\delta V_1, \delta V_2)=(-5, 10)$ mV, $\tau=16$ ns, and $B=80$ mT. The rise time is 8 ns. Yellow is low, red is medium, and black is high. (b) Calculated $P(S)$ to compare to (a).

indeed vary with detuning.

The calculation in Fig. 3(b) reveals that, at large τ_m/T_1 , the oscillations along the initial detuning axis are approximately sinusoidal (i.e. peaks and dips have equal widths along the detuning axis) and that, at small τ_m/T_1 , the dips become much wider than the peaks, just as is observed in the experimental results of Fig. 3(a). Even though the corresponding features are smeared out somewhat in experiment (presumably because of decoherence effects not included in the present model), the non-sinusoidal character of the oscillations for smaller

τ_m is clear, as one can clearly see that below $\tau_m \approx 10 \mu\text{s}$ the yellow regions are wider than the black regions in Fig. 3(a).

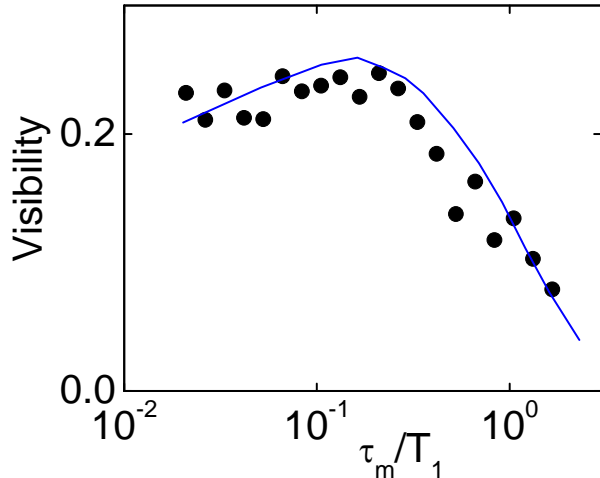


FIG. 4: (Color online) Visibility as a function of τ_m/T_1 from the experiments in Fig. 3(a), where we assume $T_1=60 \mu\text{s}$ as a fitting parameter (filled circles) and NIS calculations (blue line). Calculation parameters are the same as for the calculation in Fig. 2(a,b); in particular, $|g|\mu_B\Delta B_{xy}=0.2 \mu\text{eV}$.

VI. LZS OSCILLATION VISIBILITY

The oscillation visibility is a figure of merit with several possible definitions depending on the application. When there is little noise in the oscillations, it is possible to take the definition of visibility as $(A_{\text{max}}-A_{\text{min}})/(A_{\text{max}}+A_{\text{min}})$, where A_{max} and A_{min} are the extrema of the oscillations. In the presence of noisy oscillations requiring an average of a large number of measurements, a statistical approach based on the standard deviation is suitable to extract the visibility. In order to compare the calculation and the experiment, we use the same definition of the visibility, V , in both cases: $V = 2\sigma$, where σ is the standard deviation of $P(S)$ calculated along a given detuning trace at a fixed value of τ_m . An integral number of LZS periods are included in the visibility calculation (three in our case). We note that this definition of V would coincide with the ratio $(A_{\text{max}}-A_{\text{min}})/(A_{\text{max}}+A_{\text{min}})$ from the corresponding ideal positive sinusoidal waveforms if the noise was subtracted.

Maps such as those of Fig. 3(a) and (b) can be used to determine whether there exists an optimal value of τ_m/T_1 that maximizes the visibility. The curve for the calculated NIS visibility vs. τ_m/T_1 , shown as a solid blue line in Fig. 4, can be understood as follows. At values of $\tau_m > T_1$, spin relaxation reduces the spin-blockade signal towards zero, hence the visibility of the LZS oscillations also decreases. At τ_m much smaller than T_1 , not enough

time is spent in the measurement phase at point M for spin relaxation toward state S to occur. The projection of the qubit state vector onto the S- T_+ basis after the pulse therefore becomes the starting point for the next pulse. Even though the result may alternate statistically between $P(S)=1$ and $P(S)=0$, averaging over several pulses will lead to an overall $P(S) \sim 1/2$ and to a reduced visibility by the same averaging process as in Fig. 2(b) (the standard deviation for the NIS case is smaller than that for the IS case). For the given experimental conditions (*i.e.* for specific interdot couplings), the calculated optimum visibility occurs at a ratio $\tau_m/T_1 \sim 0.2$.

Experimentally, the visibility is also extracted as 2σ over three peaks of each detuning trace from Fig. 3(a). The results are plotted as filled circles in Fig. 4 and match the prediction from the calculations. The visibility varies by $\sim 10\%$ depending on how many periods are included in the visibility calculations because the amplitude varies with detuning as discussed above. The optimum predicted theoretically is observed at $\tau_m/T_1 \sim 0.2$, assuming $T_1=60 \mu\text{s}$ as a fitting parameter for the case presented in Fig. 4.

VII. DISCUSSION OF EFFECTS DUE TO DYNAMICAL NUCLEAR POLARIZATION

Our calculations indicate surprisingly that it is possible for the visibility obtained for IS to be less than that obtained in the statistical way for NIS. Figure 5(a) shows the calculated visibilities V obtained for the IS and NIS cases as a function of the $|g|\mu_B\Delta B_{x,y}$ hyperfine splitting responsible for the S- T_+ anticrossing. Since the value of P_{LZ} strongly influences the magnitude of the $P(S)$ oscillations and the subsequent averaged NIS visibility and P_{LZ} is directly modified by the hyperfine splitting, we would expect to see significant variations of the visibility with the splitting. For smaller splittings than usually occur in our experiments, the two curves cross and the NIS visibility is actually larger than that of IS. The calculated $P(S)$ for the two cases at $|g|\mu_B\Delta B_{xy}=0.11 \mu\text{eV}$ are shown in Fig. 5(b). For this hyperfine splitting P_{LZ} increases beyond 98% at detunings greater than -7 mV leading to $P(S)$ oscillations that are much reduced relative to Fig. 2(b). In the NIS case, the averaged minima are pulled down toward 0.5 leading to enhanced visibility. In summary, the visibility of LZS oscillations does not necessarily increase due to standard initialization (it depends on the specific experimental situation).

The visibility and the relaxation time can both be affected by dynamical nuclear polarization (DNP). The interplay between visibility, relaxation time, and pulse rise time has been investigated recently in a DQD, where DNP pulses were applied to increase the value of ΔB_z due to hyperfine nuclear interaction.²⁵ Even though we do not specifically apply a DNP pulse sequence here prior to the qubit manipulation pulse, we know from Ref.⁶ that this pulse results in a small DNP effect in our samples.

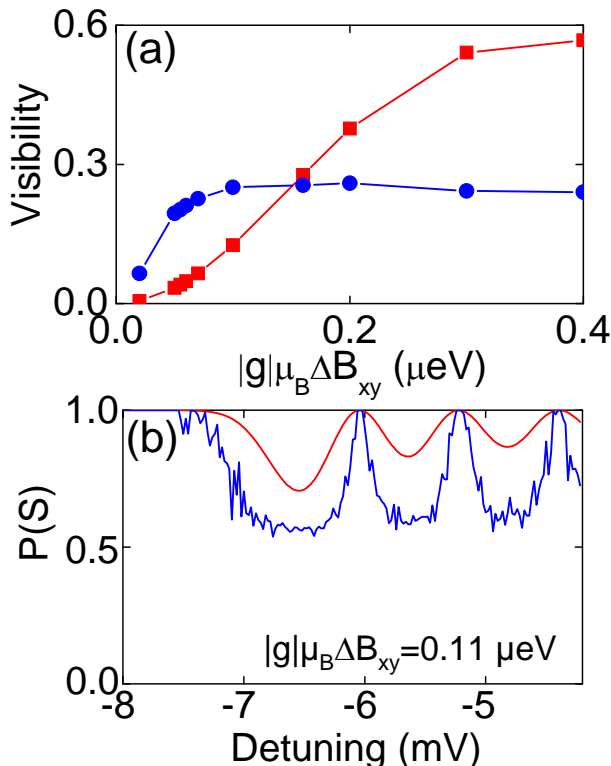


FIG. 5: (Color online) (a) Calculated IS (red squares) and NIS (blue circles) visibility for $\tau_m/T_1 \sim 0.1$ as a function of $|g|\mu_B\Delta B_{xy}$. (b) Calculated $P(S)$ vs. initial detuning for hyperfine splitting $|g|\mu_B\Delta B_{xy} = 0.11 \mu\text{eV}$ of the IS case (red). The blue curve is the NIS case for comparison.

DNP may also account for some visible difference between experimental and theoretical graphs in Fig. 3(a) and Fig. 3(b). Even though DNP effects are beyond this

study, the presented theory correctly captures the main experimental features discussed above.

VIII. CONCLUSIONS

In conclusion, we have carried out the experimental and theoretical study of the microscopic mechanisms affecting the visibility of Landau-Zener-Stückelberg oscillations in conditions where an initialization step is difficult. The results apply to cases where one of the dots is isolated from the leads (e.g. the center dot of a triple quantum dot) or where the relaxation time T_1 is too short (as for charge qubits). Partial initialization occurs in these situations due to the T_1 relaxation process during the qubit readout step.

The visibility depends on the ratio of pulse period τ_m to the relaxation time T_1 ; it reaches a broad maximum at an optimum point, which depends on system parameters. In our experiment the LZS visibility reaches a maximum of 0.25 at the optimal $\tau_m/T_1 \sim 0.2$ in good agreement with theoretical calculations. Theoretical analysis shows that in some cases (for smaller hyperfine interactions) the visibility without initialization step can exceed the one with the initialization. It is important to find optimal settings for τ_m/T_1 that can also be used for the estimation of T_1 or the level coupling at the anticrossing.

Acknowledgments

We thank O. Kodra for programming. A.S.S. acknowledges funding from NSERC Grant No. 170844-05. G.G. acknowledges funding from the NRC-CNRS collaboration.

* Electronic address: Andrew.Sachrajda@nrc.ca

¹ R. Hanson, L. P. Kouwenhoven, J. R. Petta, S. Tarucha, L. M. K. Vandersypen, *Reviews of Modern Physics*, **79**, 1217 (2007).

² M. Pioro-Ladrière, T. Obata, Y. Tokura, Y.-S. Shin, T. Kubo, K. Yoshida, T. Taniyama, and S. Tarucha, *Nature Phys.* **4**, 776 (2008).

³ S. A. Studenikin, G. C. Aers, G. Granger, L. Gaudreau, A. Kam, P. Zawadzki, Z. R. Wasilewski, and A. S. Sachrajda, *Phys. Rev. Lett.* **108**, 226802 (2012).

⁴ S. A. Studenikin, J. Thorggrimson, G. C. Aers, A. Kam, P. Zawadzki, Z. R. Wasilewski, A. Bogan, and A. S. Sachrajda, *Appl. Phys. Lett.* **101**, 233101 (2012).

⁵ E. A. Laird, J. M. Taylor, D. P. DiVincenzo, C. M. Marcus, M. P. Hanson, and A. C. Gossard, *Phys. Rev. B* **82**, 075403 (2010).

⁶ L. Gaudreau, G. Granger, A. Kam, G. C. Aers, S. A. Studenikin, P. Zawadzki, M. Pioro-Ladrière, Z. R. Wasilewski,

A. S. Sachrajda, *Nat. Phys.* **8**, 54 (2012).

⁷ G. C. Aers, S. A. Studenikin, G. Granger, A. Kam, P. Zawadzki, Z. R. Wasilewski, and A. S. Sachrajda, *Phys. Rev. B* **86**, 045316 (2012).

⁸ S. Studenikin, G. Aers, G. Granger, L. Gaudreau, A. Kam, P. Zawadzki, Z. R. Wasilewski, A. Sachrajda, *Phys. Status Solidi C* **10**, 752 (2013).

⁹ J. Medford, J. Beil, J. M. Taylor, E. I. Rashba, H. Lu, A. C. Gossard, and C. M. Marcus, *Phys. Rev. Lett.* **111**, 050501 (2013).

¹⁰ I. van Weperen, B. D. Armstrong, E. A. Laird, J. Medford, C. M. Marcus, M. P. Hanson, A. C. Gossard, *Phys. Rev. Lett.* **107**, 030506 (2011).

¹¹ J. R. Petta, H. Lu, and A. C. Gossard, *Science* **327**, 669 (2010).

¹² P. Nalbach, J. Knörzer, and S. Ludwig, *Phys. Rev. B* **87**, 165425 (2013).

¹³ L. Landau, *Phys. Z. Sowjetunion* **2**, 46 (1932).

- ¹⁴ C. Zener, Proc. R. Soc. London, Ser. A **137**, 696 (1932).
- ¹⁵ E. C. G. Stückelberg, Helv. Phys. Acta **5**, 369 (1932).
- ¹⁶ S. N. Shevchenko, S. Ashhab, Franco Nori, Physics Reports **492**, 1 (2010).
- ¹⁷ H. Ribeiro, J. R. Petta, and G. Burkard, Phys. Rev. B **82**, 115445 (2010).
- ¹⁸ G. Burkard, Science **327**, 650 (2010).
- ¹⁹ J. Särkkä and A. Harju, New J. of Phys. **13**, 043010 (2011).
- ²⁰ L. Gaudreau, A. Kam, G. Granger, S.A. Studenikin, P. Zawadzki, and A.S. Sachrajda, Appl. Phys. Lett. **95**, 193101 (2009).
- ²¹ M. Field, C. G. Smith, M. Pepper, D. A. Ritchie, J. E. F. Frost, G. A. C. Jones, and D. G. Hasko, Phys. Rev. Lett. **70**, 1311 (1993).
- ²² K. Ono, D. G. Austing, Y. Tokura, S. Tarucha, Science **297**, 1313 (2002).
- ²³ Initialization procedures did not achieve a significant improvement in the experimental visibility and we do not show any experimental results in the IS case in this paper.
- ²⁴ J. M. Taylor, *et al.* Phys. Rev. B **76**, 035315 (2007).
- ²⁵ C. Barthel, J. Medford, H. Bluhm, A. Yacoby, C. M. Marcus, M. P. Hanson, and A. C. Gossard, Phys. Rev. B **85**, 035306 (2012).